RESEARCH ARTICLE

Key Points:
- TC simulations with and without a BL scheme are substantially different
- TC BL features are sensitive to grid spacing and choice of SGS parameterization
- Despite differences among LEP runs the net effect on TC evolution may be similar

Correspondence to:
B. W. Green,
bwg5019@psu.edu

Numerical simulations of Hurricane Katrina (2005) in the turbulent gray zone

Benjamin W. Green[1] and Fuqing Zhang[1]

[1]Department of Meteorology, Pennsylvania State University, University Park, Pennsylvania, USA

Abstract Current numerical simulations of tropical cyclones (TCs) use a horizontal grid spacing as small as $\Delta x = 10^3$ m, with all boundary layer (BL) turbulence parameterized. Eventually, TC simulations can be conducted at Large Eddy Simulation (LES) resolution, which requires Δx to fall in the inertial subrange (often $<10^2$ m) to adequately resolve the large, energy-containing eddies. Between the two lies the so-called "terra incognita" because some of the assumptions used by mesoscale models and LES to treat BL turbulence are invalid. This study performs several 4–6 h simulations of Hurricane Katrina (2005) without a BL parameterization at extremely fine Δx [333, 200, and 111 m, hereafter "Large Eddy Permitting (LEP) runs"] and compares with mesoscale simulations with BL parameterizations ($\Delta x = 3$ km, 1 km, and 333 m, hereafter "PBL runs"). There are profound differences in the hurricane BL structure between the PBL and LEP runs: the former have a deeper inflow layer and secondary eyewall formation, whereas the latter have a shallow inflow layer without a secondary eyewall. Among the LEP runs, decreased Δx yields weaker subgrid-scale vertical momentum fluxes, but the sum of subgrid-scale and "grid-scale" fluxes remain similar. There is also evidence that the size of the prevalent BL eddies depends upon Δx, suggesting that convergence to true LES has not yet been reached. Nevertheless, the similarities in the storm-scale BL structure among the LEP runs indicate that the *net effect* of the BL on the rest of the hurricane may be somewhat independent of Δx.

1. Introduction

Tropical cyclones (TCs) are among the types of weather phenomena that span a large range of spatiotemporal scales. While TC track is governed by the large-scale synoptic flow, TC intensity is impacted by (among other things) environmental vertical wind shear and moisture [e.g., *Tao and Zhang*, 2014, and references therein], fluxes of momentum and moist enthalpy across the air-sea interface [e.g., *Emanuel*, 1986, 1995; *Bryan*, 2012; *Green and Zhang*, 2013, 2014], and the transport to the free atmosphere of these fluxes by the turbulent planetary boundary layer [e.g., *Braun and Tao*, 2000; *Bao et al.*, 2012; *Bryan*, 2012]. For accurate and physically realistic numerical simulations of TCs, all of these processes must be adequately resolved, or, if necessary, parameterized. Current generation numerical weather prediction (NWP) models used to simulate TCs have a horizontal grid spacing on the order of $\Delta x = 1$ km, which is convection-permitting but unable to resolve PBL turbulence. With ever increasing computational capability, Large Eddy Simulation (LES)—which explicitly resolves the large, anisotropic, energy-containing turbulent eddies and parameterizes the small and isotropic eddies—will eventually become feasible for TC simulations. While the assumptions used by NWP models to parameterize PBL turbulence begin to fail for $\Delta x < O(1$ km), LES is questionable when the grid spacing is outside the inertial subrange [often when $\Delta x > O(100$ m)]; the resulting "gap" between LES and mesoscale simulations is often referred to as the turbulent gray zone or "terra incognita" [*Wyngaard*, 2004].

To date, only a handful of TC simulations have been run with $\Delta x < 1$ km. *Nolan et al.* [2009a, 2009b] and *Wang* [2014] had innermost grid meshes of 444 and 250 m, respectively, all of which used a PBL parameterization scheme. *Zhu* [2008] used a PBL scheme for domains with $\Delta x \geq 900$ m; the PBL scheme was turned off and replaced by a 3-D Smagorinsky subgrid-scale (SGS) scheme for the 300 and 100 m domains (which only comprises a small subregion of the TC's inner core). *Rotunno et al.* [2009]—whose domains were centered on the TC vortex—parameterized SGS fluxes in their subkilometer meshes by a grid-spacing-dependent turbulence kinetic energy (TKE) method and found a sharp increase in randomly distributed small-scale turbulent eddies when Δx was decreased from 185 to 62 m. If $\Delta x = 62$ m represents the upper limit on the grid spacing necessary for TC LES, widespread implementation remains many years away. Another set of idealized TC LES experiments [*Bryan et al.*, 2014; *Stern and Bryan*, 2014; *Rotunno and Bryan*,

Table 1. Summary of Model Configuration for Each Simulation

Experiment Name	PBL/SGS Scheme	Δx (m)	Δt (s)	Horizontal Domain Size (Grid Points)	Parent Domain	Start Time
YSU3k	YSU PBL	3000	20/3	757×757	See text	1200 UTC
YSU1k	YSU PBL	1000	20/9	1000×1000	YSU3k	1200 UTC
MYNN1k	MYNN PBL	1000	20/9	1000×1000	YSU3k	1200 UTC
YSU333	YSU PBL	333.3333	20/27	2449×2449	YSU1k	1200 UTC
LEP333	NBA SGS	333.3333	20/27	2449×2449	YSU1k	1200 UTC
LEP200	NBA SGS	200	20/45	2356×2356	YSU1k	1200 UTC
LEP111	NBA SGS	111.1111	20/81	2503×2506	LEP333	1400 UTC

2014] was run with $\Delta x = 62$ m and used a "two-part" SGS model [*Sullivan et al.*, 1994]; it should be noted that because TCs are quite spatially heterogeneous, temporal averages were used in lieu of spatial averages—an issue that will be discussed later in this paper.

In the meantime, to avoid the prohibitive costs of TC-wide LES, there have been highly idealized LES studies of the TC boundary layer [*Nakanishi and Niino*, 2012; *Green and Zhang*, 2015]. Out of necessity, these simulations used periodic lateral boundary conditions for a horizontally homogeneous domain valid at a single radius dozens of km from TC center. While these studies provide insight into the strongly sheared, rapidly rotating boundary layer that is characteristic of a TC, *Green and Zhang* [2015] note that such an idealized LES configuration cannot capture either mesoscale radial gradients or net vertical velocities, both of which are key aspects of real TCs [e.g., *Kepert and Wang*, 2001].

Since the publication of *Rotunno et al.* [2009], the Weather Research and Forecasting (WRF) model [*Skamarock et al.*, 2008] has incorporated a new SGS parameterization scheme—the nonlinear backscatter with anisotropy (NBA) scheme [*Mirocha et al.*, 2010]—that, at coarser resolutions, performs much better than the Smagorinsky and TKE SGS schemes (a caveat is that the NBA scheme was only validated for a neutral boundary layer with shear-driven turbulence. Turbulent eddies in TCs are both shear-driven and buoyancy-driven; buoyancy is particularly important in the eyewall convection (P. Zhu, personal communication, 2014). The development of the NBA SGS scheme, coupled with the increase in computing power over the past 5 years, presents a great opportunity to revisit the problem of simulating TCs at Δx between 10^2 and 10^3 m.

This study is the first to simulate the inner core of a real TC (in this case, 2005 Hurricane Katrina) *without a PBL scheme* at Δx as small as 111 m. In doing so, we aim to address some outstanding questions regarding the simulation of TCs at subkilometer scales. One, what are the differences in TC intensity and structure between mesoscale runs (using a PBL scheme) and "Large Eddy Permitting (LEP)" runs (using the NBA SGS)? And two, are there signs of convergence toward true LES at $\Delta x = 111$ m?

The remainder of this paper is organized as follows. Section 2 details the experimental design. Results are presented in section 3. A discussion can be found in section 4, followed by concluding remarks in section 5.

2. Experimental Design

Version 3.4.0 of the Advanced Research WRF (WRF-ARW) was used to simulate Hurricane Katrina (2005). Identical to *Green and Zhang* [2013], a 60 member ensemble was initialized at 0000 UTC 25 August 2005 and integrated forward for 14.5 h. From 1430 UTC to 2000 UTC, six rounds of airborne Doppler radar velocity data were assimilated by an ensemble Kalman filter [*Weng and Zhang*, 2012]. At 2000 UTC, the mean of the 60 ensemble members (for each of the three domains—27, 9, and 3 km) was integrated forward until 1200 UTC 28 August 2005. The relevant model physics used during this time were the Yonsei University (YSU) PBL scheme [*Hong et al.*, 2006] with surface layer momentum fluxes calculated from *Donelan et al.* [2004] ("Opt 2" in *Green and Zhang* [2013]). Additional details on this part of the model configuration can be found in section 3 of *Green and Zhang* [2013]. As described below and summarized in Table 1, several one-way nested simulations—both with and without PBL schemes—were run between 1200 UTC and 1800 UTC 28 August. The number of vertical levels was increased to 85 to provide finer resolution near the surface: specifically, the first model level is at a height of approximately 17 m; vertical grid spacing gradually increases to $\Delta z \approx 111$ m at a height of $\sim$1.2 km (model level 19). Above a height of $\sim$5 km, vertical grid spacing ranges between 300 and 400 m. All of the one-way nested domains were fixed in space (that is, they were not vortex-following). Unfortunately, because writing out such large data sets is extremely computationally expensive, output was only saved every hour.

2.1. Simulations Using a PBL Scheme

A total of four simulations were run from 1200 UTC to 1800 UTC with a PBL scheme. One, hereafter "YSU3k," used the YSU PBL scheme with $\Delta x = 3$ km, a time step of 20/3 s, and a horizontal domain of 757×757 grid points. The second ("YSU1k") was initialized from YSU3k at 1200 UTC, used the YSU scheme with $\Delta x = 1$ km, a time step of 20/9 s, and a horizontal domain of 1000×1000 points. The third ("YSU333") was initialized from YSU1k at 1200 UTC, used the YSU PBL scheme with $\Delta x = 333.3333$ m, a time step of 20/27 s, and a horizontal domain of 2449×2449 points. Finally, to examine the sensitivity to choice of PBL scheme, a fourth simulation ("MYNN1k") was run with the same configuration as YSU1k except for the use of the MYNN PBL scheme [*Nakanishi and Niino*, 2004].

2.2. Simulations Using the NBA SGS Scheme

Three simulations—all with $\Delta x < 1$ km—were run without a PBL scheme to determine if the NBA SGS could produce features resembling turbulent eddies in the "terra incognita" range. Two of these simulations, termed "LEP333" ($\Delta x = 333.3333$ m) and "LEP200" ($\Delta x = 200$ m), were initialized at 1200 UTC directly from the YSU1k simulation with respective time steps of 20/27 and 20/45 s. The highest-resolution simulation, "LEP111" ($\Delta x = 111.1111$ m), was initialized from LEP333 at 1400 UTC because the computational demands of this simulation (horizontal grid size of 2503×2506 points and time step of 20/81 s). The lateral boundary conditions for the nested runs were provided by the parent domain (see Table 1).

3. Results

To exemplify the differences and similarities between PBL and LEP simulations, a compilation of simulated visible satellite imagery (as derived from the short-wave radiation reaching the surface, or SWDOWN field) for four of the simulations valid at 1800 UTC 28 August—YSU1k, YSU333, LEP333, and LEP111—is shown in Figure 1. The LEP333 and LEP111 runs (Figures 1c and 1d) show, for the first time, subkilometer simulations without a PBL scheme of a real TC over such a large spatial extent. All simulations exhibit very large polygonal eyes with low-level clouds, and the LEP111 run in particular exhibits a stunning amount of detail. But these simulated visible satellite images only represent the vertically integrated effects of clouds; in this paper, we will focus on TC characteristics within the boundary layer.

3.1. Near-Surface Thermodynamic Structure

To get a sense of the low-level thermodynamic structure of the simulated TCs, Figure 2 shows the distribution of potential temperature θ (valid at 1800 UTC) as diagnosed from the surface layer scheme. In addition to the three YSU runs and three LEP runs, Figure 2 also shows (bottom row) the LEP runs regridded to $\Delta x = 1$ km. The regridding was performed by partitioning each of the LEP domains into 1×1 km boxes and then taking the average of all points within each box. Some form of regridding, or down-filtering, was suggested by *Bryan et al.* [2003, p. 2400] as "a more appropriate comparison… [to] better address the question of whether [different] resolutions are producing equivalent structures." Looking at Figure 2, there are several noteworthy features. First, there is a strong gradient in 2 m θ between the eye and eyewall, approaching 15 K; part of this difference is due to the change in surface pressure, but the 2 m *temperature* field still shows eye-eyewall differences of 5–10 K (not shown). Second, the LEP runs (Figures 2d–2f) produce finer-scale structures than the YSU runs (Figures 2a–2c), even when comparing on a common grid mesh (cf. Figure 2c with Figure 2d and Figure 2b with Figures 2g–2i). Indeed, the NBA SGS used in the LEP runs appears to encourage the development of roll-like structures. Furthermore, while finer-scale features are evident with increasing horizontal resolution in the LEP runs (cf. Figures 2d–2f), filtering to a common 1 km grid (Figures 2g–2i) shows that the storm-scale features are more or less the same—except for the shape of the polygonal eyewall. In fact, all simulations (at 1800 UTC) exhibit polygonal eyewalls of various shape and orientation, which is remarkable because these runs have only been integrated independently for 6 h (4 h in the case of LEP111); thus, polygonal eyewall structure and evolution is sensitive to BL parameterization (or lack thereof) and horizontal grid spacing.

3.2. Distribution of 10 m Wind Speeds and "Point Metrics" of Intensity
3.2.1. Spatial Structures of 10 m Wind Field

Figure 3 is similar to Figure 2 except that distributions of 10 m wind speed are shown in a 100×100 km box around the TC center. It is important to note how TC center was calculated, given the sensitivity of
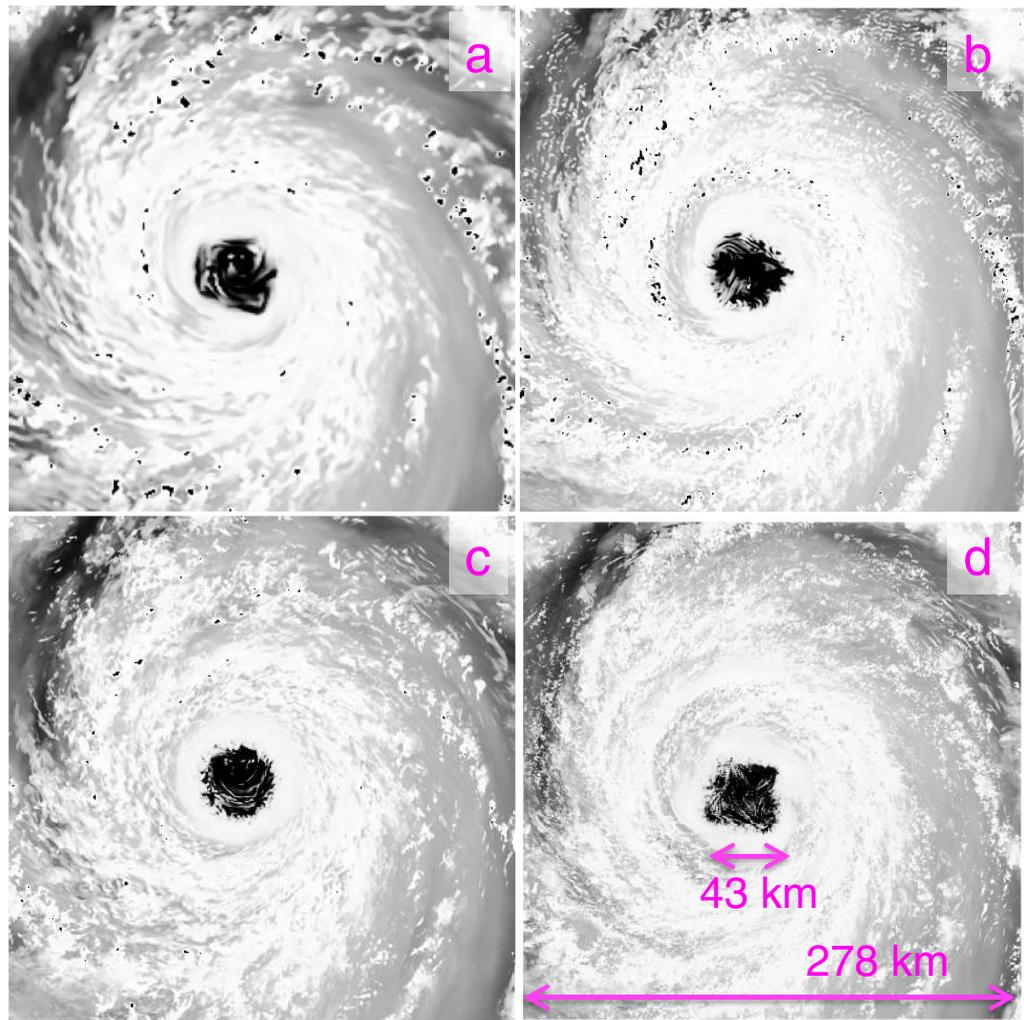
Figure 1. Simulated visible satellite images (based on the short-wave radiation reaching the ground, or SWDOWN field in WRF) valid 1800 UTC 28 August 2005 for (a) YSU1k, (b) YSU333, (c) LEP333, and (d) LEP111. Domain size is equal in all four panels.

various objective methods [*Ryglicki and Hart*, 2014]; here, we ran a nine-point smoother for 5000 iterations on the sea level pressure (SLP) field and defined the center as the location of the minimum of the smoothed SLP. Reassuringly, the same spatial patterns evident in Figure 2 are also evident in Figure 3. More importantly, Figure 3 can be directly compared with Figure 2 of *Rotunno et al.* [2009]. Unlike *Rotunno et al.* [2009]—which only found small, randomly distributed pockets of extreme wind speeds at $\Delta x = 62$ m (their Figure 2d)—we find such fine-scale features in all of our LEP runs (Figures 2d–2f), even as coarse as $\Delta x = 333$ m. It is possible that this difference is due to the choice of SGS scheme; *Mirocha et al.* [2010] demonstrated that the NBA scheme (used in this study) performs better at larger Δx (i.e., coarser LEP runs) than the TKE-based scheme used by *Rotunno et al.* [2009].

3.2.2. Intensity Point Metrics

Many numerical studies of TCs present the storm intensity in terms of the so-called "point metrics" of minimum SLP and maximum 10 m wind speed. Here we show how the point metrics vary between the different simulations. Looking at Figure 4a, the runs fall into three categories in terms of minimum SLP: the PBL runs with $\Delta x \geq 1$ km have the highest pressures, followed by the LEP runs, and finally YSU333.

The hourly evolutions of instantaneous maximum 10 m wind speed are shown in Figure 4b. Here the mesoscale runs with $\Delta x \geq 1$ km exhibit much weaker wind speeds (on the order of 10–25 m s^{-1}) than YSU333 and all of the LEP runs. This is not surprising at all because the LEP runs are beginning to resolve
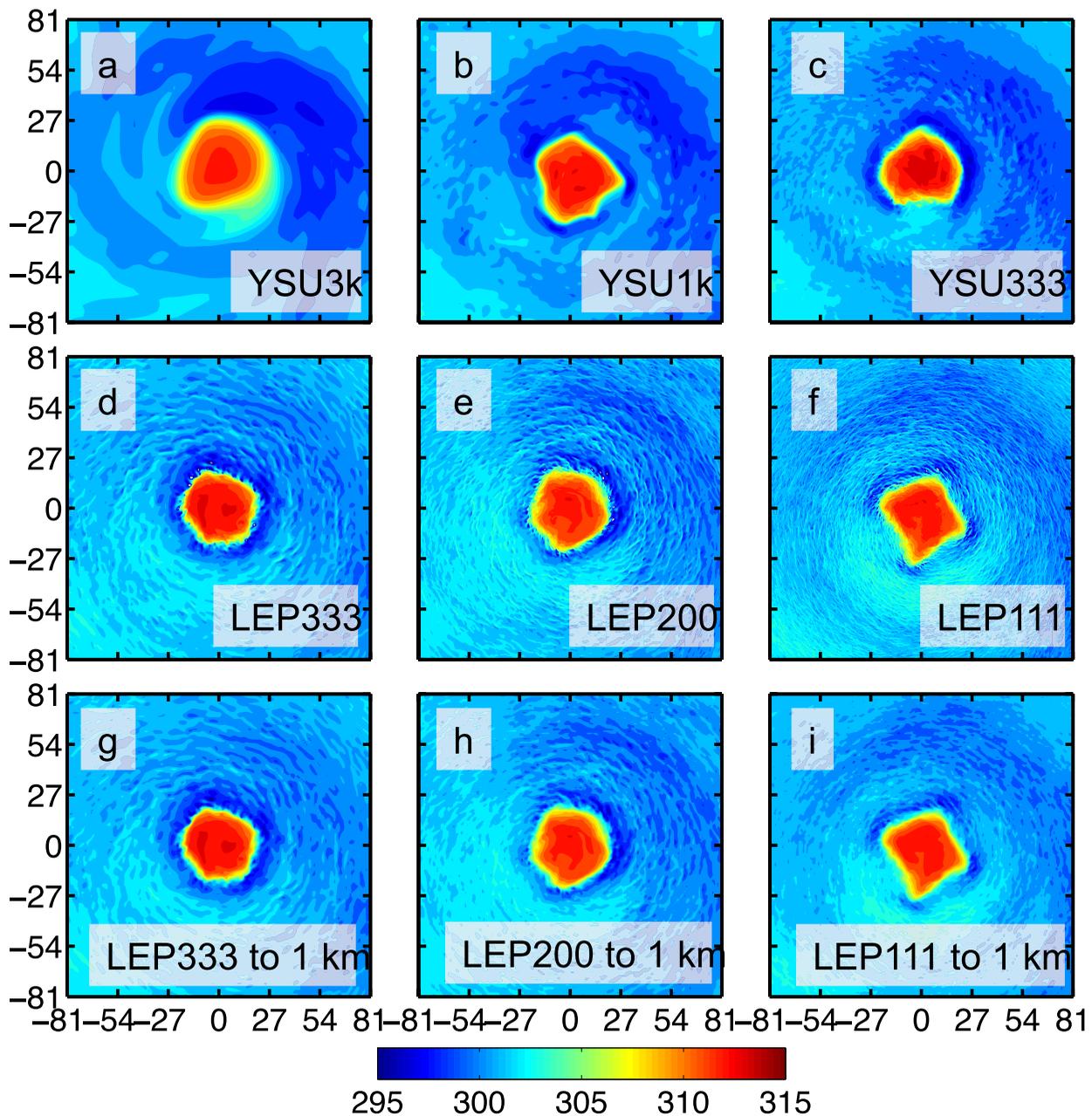
Figure 2. Plots of 2 m potential temperature (in K) valid 1800 UTC 28 August 2005 for (a) YSU3k, (b) YSU1k, (c) YSU333, (d) LEP333, (e) LEP200, and (f) LEP111. In Figures 2g–2i, the LEP333, LEP200, and LEP111 runs, respectively, have been filtered to a grid with $\Delta x = 1$ km. Tick marks represent distance (in km) from TC center.

turbulence—that is, transient eddies or *wind gusts*—that are much stronger than the mean flow. Such a result is in agreement with *Nolan et al.* [2009a, p. 3665], who state that the minimum Δx "for which instantaneous winds are a good representation of 1 min averages [used for best track] appears to be somewhere around 1 km." As regional-scale NWP models begin to move toward $\Delta x < 1$ km, verification of TC intensity would be more appropriate using output 1 min averages. Because our simulations did not output 1 min averages of 10 m wind speed, we show instead in Figure 4c the instantaneous maximum 10 m winds after filtering to a common 1 km grid. By down-filtering to 1 km, the strongest winds are now 10–20 m s^{-1} weaker and are much more in line with the coarser PBL runs (YSU1k and MYNN1k). Interestingly, the down-filtered results show a pattern amongst the LEP runs—maximum 10 m wind speed decreases with decreasing Δx.
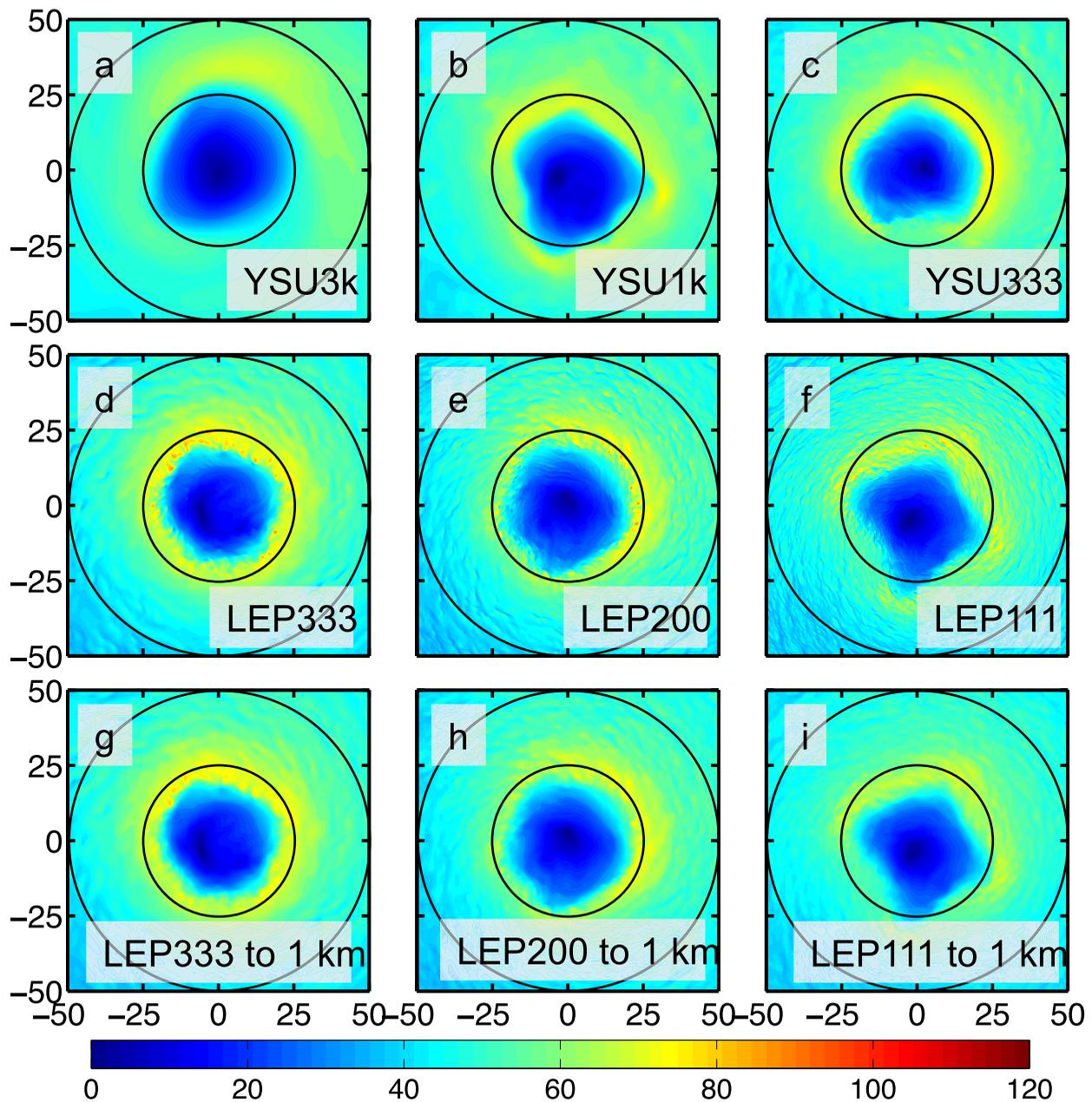
Figure 3. As in Figure 2, but for 10 m wind speed (in m s^{-1}). Range rings are drawn at 25 and 50 km from TC center.

3.2.3. Statistical Distribution of 10 m Wind Speed

One way to expand on the results of Figures 4b and 4c is to look at the empirical cumulative distribution functions (CDF) of the 10 m wind speeds; Figure 5 does just that, for a 162 × 162 km horizontal box centered around the TC vortex (valid at 1800 UTC). Looking at Figure 5a, there is a subtle—but distinct—difference between the LEP and PBL runs: the former have a higher fraction of points with wind speeds below 50 m s^{-1}. Another way to interpret this result is that the PBL runs have a sharper "peak" in the empirical probability density function for wind speeds between 30 and 60 m s^{-1}.

The right tail of the wind speed distributions is highlighted in Figure 5b. There are several items worthy of note here. First, the (1-CDF) curves for the PBL runs all decline very sharply just before the maximum 10 m wind speed is reached; in other words, there is a relatively large number of points with wind speeds that are *just*
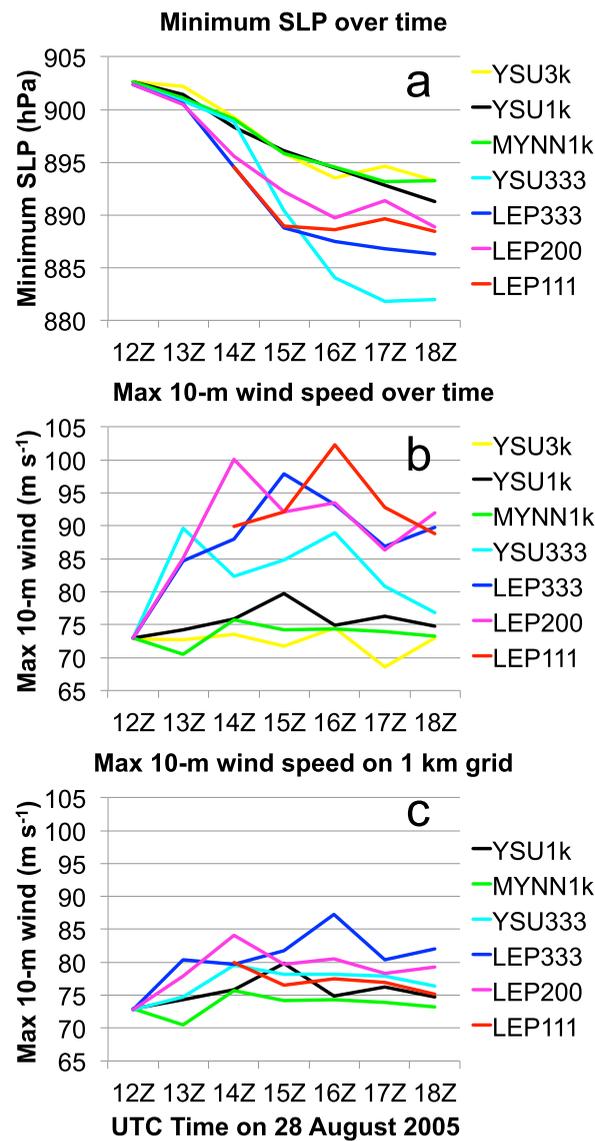
Figure 4. Temporal evolution of "point metrics" of TC intensity for the various runs. (a) Minimum SLP (in hPa). (b) Instantaneous maximum 10 m wind speed (in m s^{-1}). (c) As in Figure 4b, but after runs have been filtered to a common horizontal grid of $\Delta x = 1$ km.

weaker than the absolute maximum. One way to interpret this result is that PBL schemes (including the MYNN1k, which is not shown for graphic clarity) are discouraging the development of very strong, very localized transient wind gusts. This may be desirable for mesoscale simulations with $\Delta x \geq 1$ km, which are intended to only represent the mean flow, but obviously a problem once turbulent eddies start to become explicitly resolved in subkilometer runs. In contrast with the PBL runs, the LEP runs on the original fine-resolution grids (that is, not down-filtered to $\Delta x = 1$ km; solid lines in Figure 5b) do not exhibit steep declines in the (1-CDF) curves (cf. YSU333 versus LEP333), which means that the NBA SGS is allowing strong, localized *turbulent gusts* to develop. When the subkilometer runs are all filtered to a 1 km grid (dashed lines), two more key results emerge. One, the tail of the YSU333 wind speed CDF remains essentially unchanged, lending support to the notion that PBL schemes are discouraging the formation of small and localized wind gusts. Two, the (filtered) LEP output confirms what was suggested at the end of the previous subsection: that the winds at the tail of the distribution *weaken* with decreasing Δx. This is evidence that the size of the prevailing turbulent eddies in these LEP runs are grid-size-dependent: on a coarser grid (e.g., LEP333), the eddies are larger in size than on a finer grid (LEP111). Indeed, this is qualitatively evident in Figure 3 (cf. Figure 3d with Figure 3f).

3.3. Energy Spectra of Vertical Velocity

Another way to examine the dependence on grid resolution and to assess the degree of convergence toward LES is to conduct a spectral analysis. In Figure 6, we present the results from spectral analyses over the horizontal domain (162 × 162 km) in Figure 2 but for vertical velocity w at WRF sigma levels with heights of approximately 172, 507, 1011, and 2069 m. Following *Bryan et al.* [2003], we have highlighted scales greater than $6\Delta x$ (at smaller scales, "unphysical" solutions arise because of numerical diffusion).

Because the strength of the eyewall updraft increases with height in the lowest 2 km (not shown), the amount of energy at larger wavelengths (i.e., vortex scale) increases with height in Figure 6. In the lower part of the boundary layer (below 1 km, Figures 6a and 6b), there is clear separation between the different runs at smaller wavelengths, both in magnitude and location of the spectral "peak." Interestingly, all of the simulations with $\Delta x < 1$ km—even YSU333—show a spectral range where the w spectrum follows a $-5/3$ power law, which indicates that an inertial subrange is present in these runs [e.g., *Bryan et al.*, 2003]. At all levels shown, the spectral "peak"—which indicates the prevailing large eddy size ℓ—shifts to the right with decreasing Δx. Therefore, the characteristics of the turbulence are dependent on Δx, which is consistent
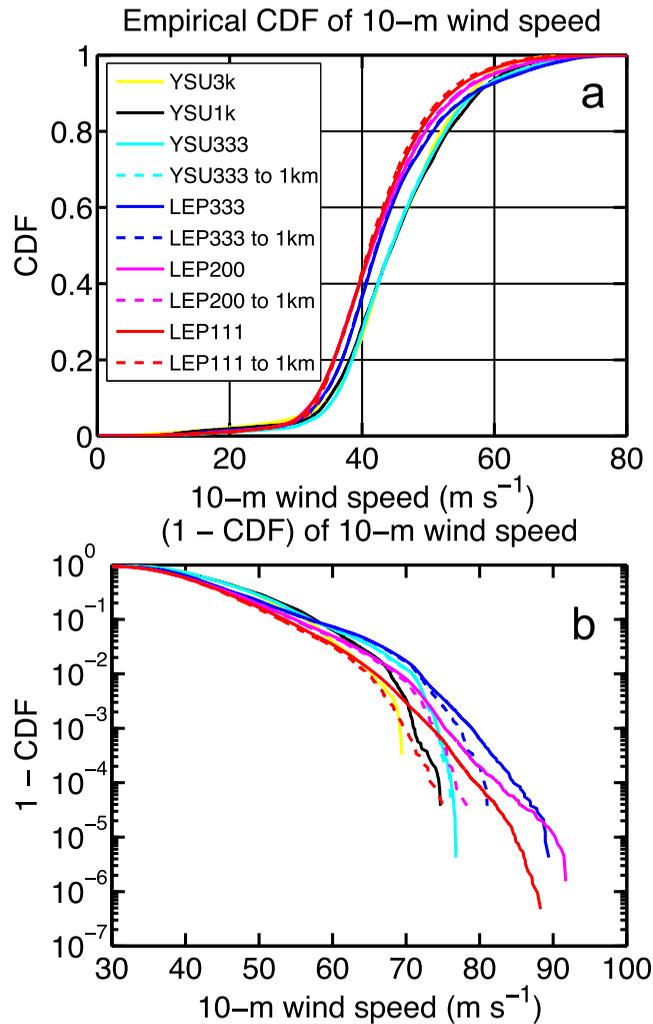
Figure 5. (a) Empirical cumulative distribution function (CDF) of 10 m wind speed (over a 162 × 162 km box centered on the TC vortex, cf. Figure 2) valid at 1800 UTC 28 August 2005 for different simulations; dashed lines are for simulations filtered to $\Delta x = 1$ km. (b) Similar to Figure 5a, but for 1-CDF.

with the qualitative assessment of Figures 2 and 3. Given the ratio between ℓ and Δx is on the order of 10, these LEP simulations likely have *not* shown convergence toward true LES (*Bryan et al.* [2003] found a similar ratio of $\ell/\Delta x \sim 10$ in their simulations, but argued that $\ell/\Delta x$ should be on the order of 100). Nevertheless, it is still worthwhile to further investigate the differences between the PBL runs and the LEP runs, particularly the BL structure in the azimuthally averaged radius-height sense.

3.4. Azimuthally Averaged TC Characteristics

The dynamics and structure of TCs are often examined in an axisymmetric framework, that is, after taking azimuthal averages. While such an approach will be followed here, it is necessary to remind the reader that issues with axisymmetric analyses can arise when the TC exhibits strong asymmetries—particularly if the eye is polygonal. To illustrate this, range rings of 25 and 50 km from the smoothed TC center (see above) are plotted in Figure 3. In some cases—particularly YSU1k (Figure 3b) and LEP111 (Figures 3f and 3i)—the polygonal eye means that, for some radii, there are locations inside the eye (south side of LEP111) and other locations within
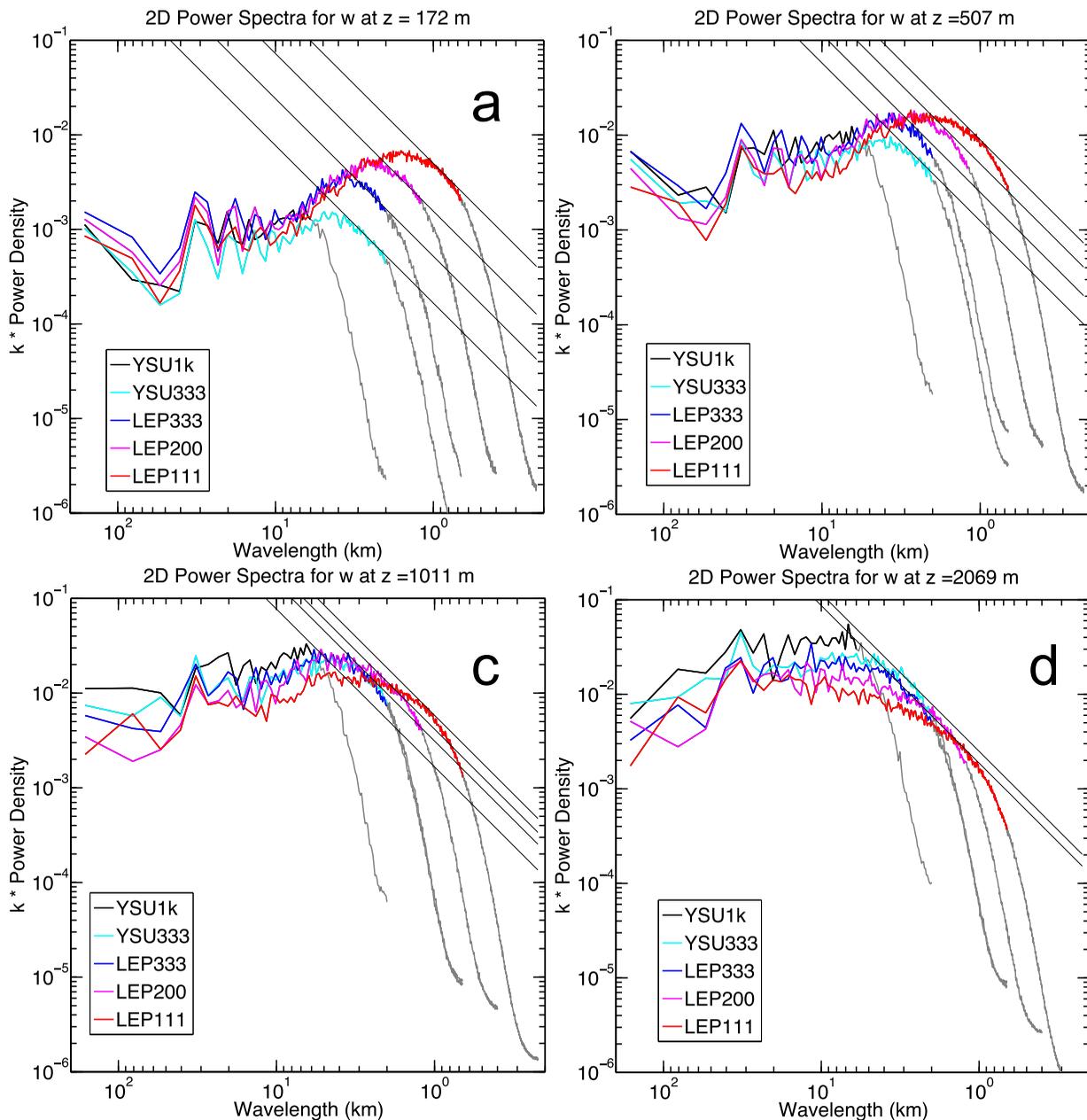
the eyewall (north side of LEP111). Therefore, when taking the azimuthal average, there will be considerable variance in the wind and a weaker *average* wind that is not representative of the winds in the polygonal eyewall. In Figure 7, the azimuthal average, and standard deviation, of the tangential wind (as functions of height and radius) are shown for each LEP run at 1400 UTC, 1600 UTC, and 1800 UTC 28 August. As expected, LEP111—with a prominent and distorted polygonal eye [at 1600 UTC (not shown), the eye of LEP111 is similarly misshapen]—has a weaker azimuthally averaged tangential wind and considerably larger standard deviation than both LEP333 and LEP200 in the vicinity of the eyewall (15–30 km). Consequently, the differences between the LEP runs for azimuthally averaged fields between 15 and 30 km (discussed below) are best explained by eyewall asymmetry.

Besides differences in eye shape, there are some consistent structural differences between the PBL runs and the LEP runs. Figure 8 shows the maximum tangential and radial wind as functions of radius for all runs but YSU3k. Here all data were first filtered to a common 1 km grid before azimuthal averages were calculated. By 1600 UTC (Figures 8b and 8e), the three PBL runs (MYNN1k, YSU1k, and YSU333) all show signs of developing a secondary wind maximum (between 50 and 60 km) in both the tangential and radial components. By 1800 UTC, the PBL runs all have a secondary peak in the tangential wind (Figure 8c); more profound, however, is that the *strongest* radial inflow of the PBL runs is no longer at the primary eyewall but at a radius of around 60 km (Figure 8f). In contrast, the filtered LEP runs do not exhibit a secondary peak in

Figure 6. Energy spectra (as a function of wavelength, in km) of vertical velocity *w* valid at 1800 UTC 28 August 2005 for various simulations at heights of approximately (a) 172, (b) 507, (c) 1011, and (d) 2069 m. Wavelengths less than 6Δx (where numerical diffusion may be producing unrealistic spectra) have been colored differently (thick gray curves). Thin lines show a −5/3 slope for reference.

either the tangential or the radial wind field. This is clear evidence that switching from a PBL parameterization scheme to the LEP, which only parameterizes SGS fluxes via the NBA scheme, significantly impacts the TC's boundary layer structure and thus the storm's future evolution.

3.4.1. Secondary Circulation as a Function of Radius and Height
Because the boundary layer frictional process is one of the most important driving mechanisms for the secondary circulation of a TC, we now look at how the low-level secondary circulation (in and up) varies between the simulations. Figure 9 compares the PBL simulations with Δx ≥ 1 km. In this short time (6 h), there are some differences between YSU3k and YSU1k (Figures 9a–9c), namely that YSU3k has a stronger inflow (and return outflow) outside of the primary eyewall, whereas YSU1k has a stronger inflow/outflow at
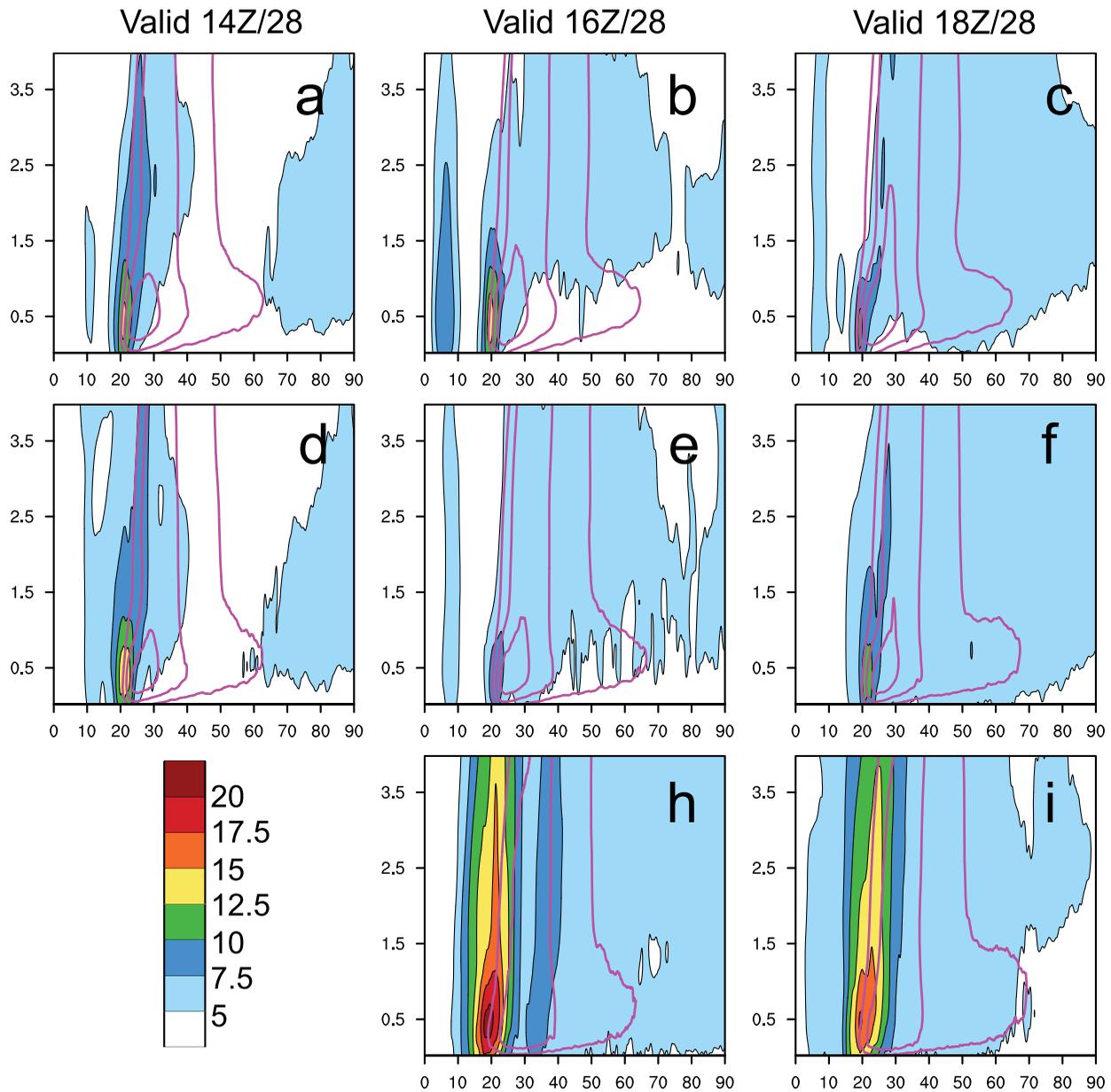
Figure 7. Radius-height plots (x and y axes, respectively, in km) of azimuthally averaged tangential wind (pink contours every 10 m s^{-1} starting at 60 m s^{-1}) and azimuthal standard deviation of tangential wind (color fill, in m s^{-1}) for (top) LEP333, (middle) LEP200, and (bottom) LEP111. Left, middle, and right columns are valid at 1400 UTC, 1600 UTC, and 1800 UTC 28 August 2005, respectively.

the primary eyewall. The only difference between YSU1k and MYNN1k is that the former has a stronger secondary circulation (Figures 9d–9f). Importantly, all PBL runs develop a clear secondary convergence zone, with a concomitant mesoscale updraft exceeding 1 m s^{-1}.

The transition from parameterized turbulence to partially resolved turbulence is shown in Figure 10. Compared with Figure 9, the differences in going from 1 km to 333 m and turning off the PBL scheme (Figures 10a–10c) are far greater than those amongst the different PBL runs. Specifically, going from YSU1k to LEP333 means a stronger, more shallow inflow layer without any sign of secondary eyewall formation. But which is more important: going from 1 km to 333 m, or turning off the PBL scheme? Figures 10d–10f show the differences between LEP333 and YSU333 (that is, the effect of turning off the PBL scheme) whereas Figures 10g–10i show the differences between YSU1k and YSU333 (the impact of changing Δx). Although the
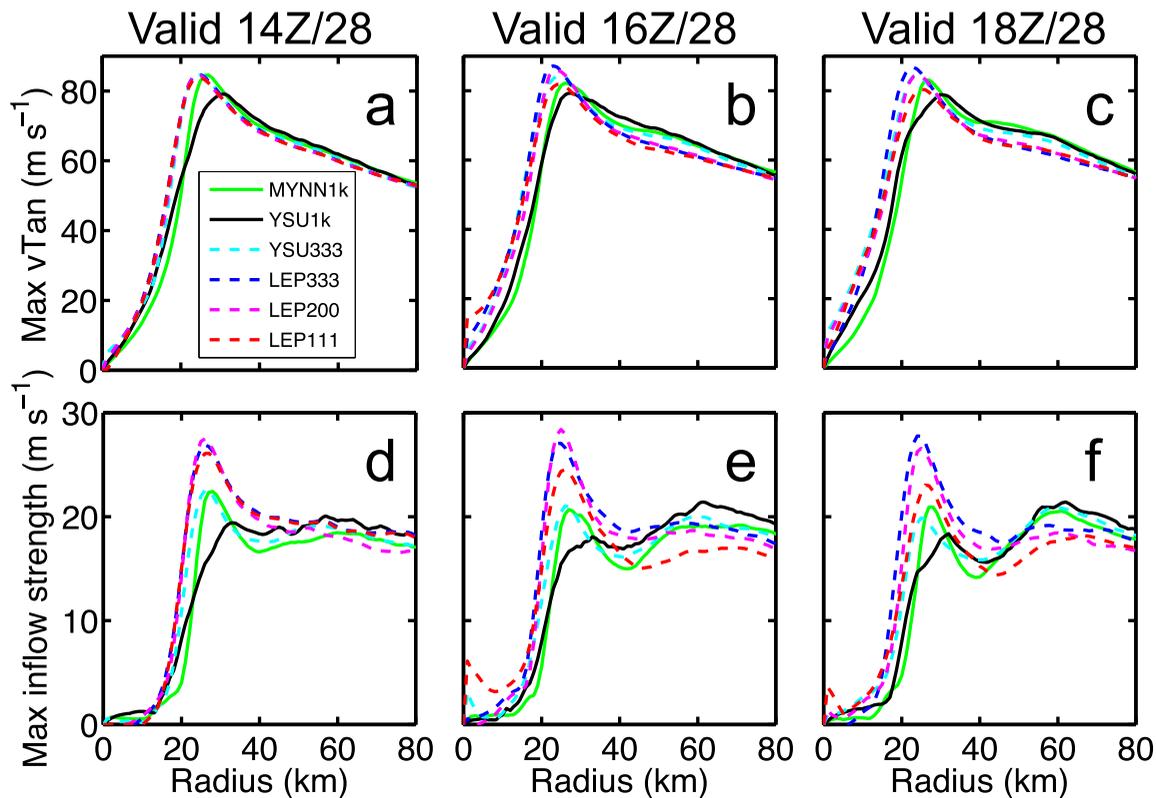
Figure 8. Plots as functions of radius of Figures 8a–8c maximum tangential wind and Figures 8d–8f maximum low-level inflow valid at (left) 1400 UTC, (middle) 1600 UTC, and (right) 1800 UTC 28 August 2005. All runs have been filtered to a common grid of $\Delta x = 1$ km.

two separate effects are not exactly additive due to the nonlinearity of the dynamics, it is clear that turning off the PBL scheme is far more important than decreasing the grid spacing: YSU333 also shows signs of secondary eyewall formation and is much more similar to YSU1k than it is to LEP333. The question then becomes, do the LEP runs with finer resolutions behave similarly to LEP333?

To answer that question, Figure 11 compares the secondary circulation of all the LEP runs. Before proceeding further, recall that LEP111 has a highly irregular polygonal eye and thus will have more "diffuse" (i.e., weaker) azimuthal averages at radii between 15 and 30 km (cf. Figure 7). Ignoring this region, the differences between the LEP runs are quite minor relative to those shown in Figures 9 and 10: LEP333 has a stronger inflow in the lowest 500 m out to a radius of ∼60 km. More importantly, though, is that *none* of the LEP runs show any sign of secondary eyewall formation. Admittedly, the development of a secondary eyewall in the PBL runs at this time was fortuitous, but the fact that the LEP runs *did not* develop a secondary eyewall shows just how important the boundary layer is for secondary eyewall formation, consistent with a growing body of research [*Fang and Zhang*, 2012; *Kepert*, 2013; *Wang et al.*, 2013].

3.4.2. Boundary Layer Momentum Fluxes
The key difference between the PBL and LEP simulations in this study is how turbulent fluxes (especially in the boundary layer) are handled. In mesoscale NWP models that use PBL schemes, it is assumed that none of the turbulence is resolved and thus all of it must be parameterized [*Wyngaard*, 2004]. In LES, however, the anisotropic, energy-containing eddies are supposed to be explicitly resolved, and only the small isotropic eddies are left to be parameterized. In fact, one way to determine if the grid spacing of an LES run is adequately resolving the large, energy-containing, anisotropic eddies is to compare the vertical profiles of the resolved and SGS turbulent momentum fluxes. If the SGS fluxes dominate the resolved fluxes in the lowest part of the boundary layer and are near zero above, then the simulation is adequately resolving the large eddies; otherwise, the simulation is not truly LES.
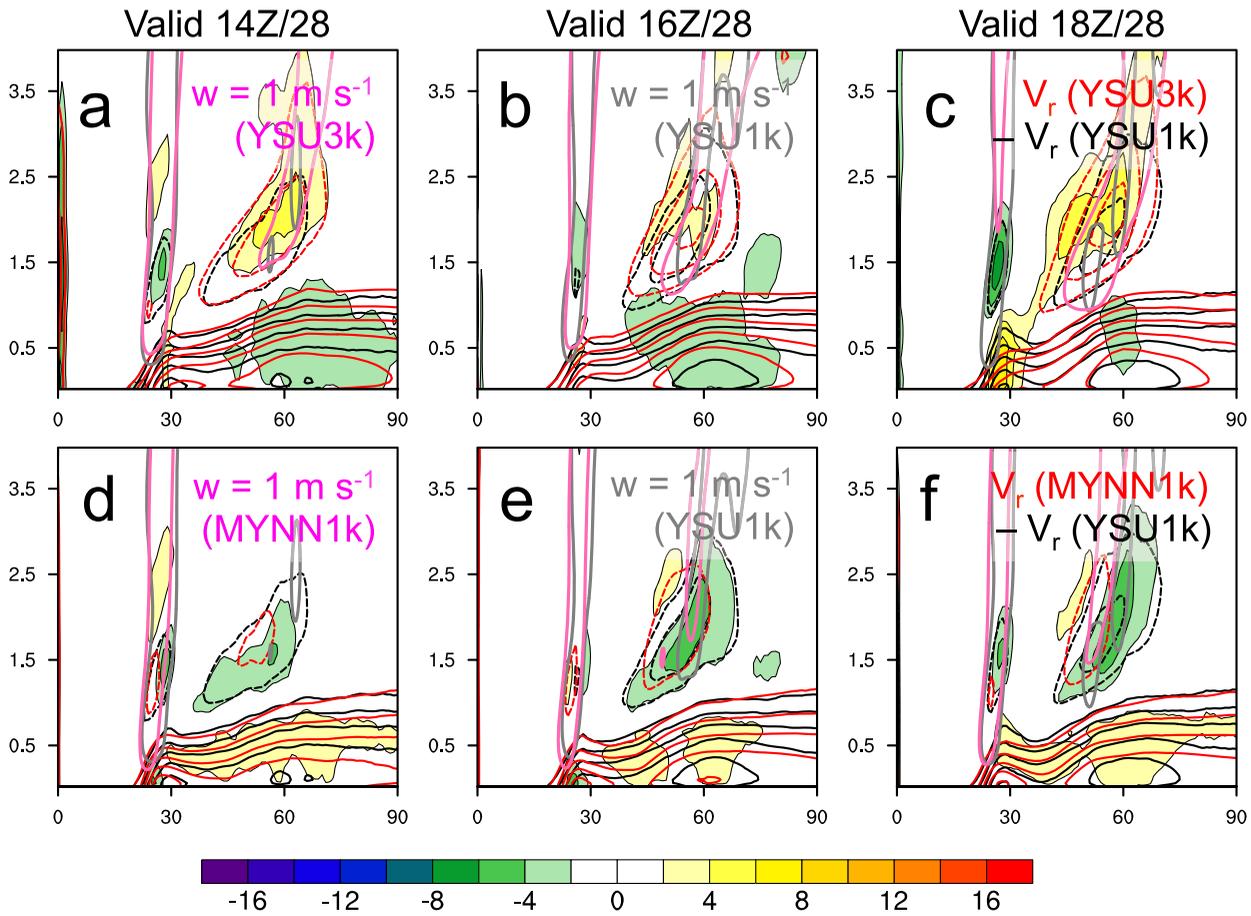
Figure 9. Radius-height plots (tick marks in km) of low-level secondary circulation for various PBL runs valid at (left) 1400 UTC, (middle) 1600 UTC, and (right) 1800 UTC 28 August 2005. Radial wind V_r is contoured (red and black) every 4 m s^{-1} with zero contour omitted; solid (dashed) lines denote negative (positive) V_r. The $w = 1$ m s^{-1} updraft is also contoured (pink and gray). (a–c) YSU3k (V_r in red, w in pink) and YSU1k (V_r in black, w in gray); color fill denotes V_r (YSU3k) minus V_r (YSU1k). (d–f) As in Figures 9a–9c but for MYNN1k versus YSU1k.

The magnitude of the vertical turbulent momentum flux in Cartesian coordinates is

$$\sqrt{(\overline{u'w'})^2 + (\overline{v'w'})^2},$$

where primes denote deviations from a mean state, overbars denote a mean, and (u, v, w) are the Cartesian velocity components. Often, LES is conducted for flows with a horizontally homogeneous mean state; in such a case, the magnitude of the resolved turbulent momentum flux can be calculated using

$$\sqrt{\left(\overline{[u_R - \overline{u_R}][w_R - \overline{w_R}]}\right)^2 + \left(\overline{[v_R - \overline{v_R}][w_R - \overline{w_R}]}\right)^2},$$

where the subscript R denotes (u, v, w) velocity resolved by the LES and the overbar denotes a horizontal average over the LES domain.

One challenge of the current study is that the LES (or, more appropriately in this case, LEP) is simulating a powerful TC, with numerous strong mesoscale gradients (namely, the radial gradients in wind, cf. Figures 3 and 8). Consequently, taking a horizontal average over the entire domain would not yield representative values of the "resolved" turbulent momentum fluxes at any particular region of the TC. Instead, we will take *localized* horizontal averages—specifically, for each point on the domain, we average over an 8×8 km box centered on that point. The choice of averaging size (8 km to a side) is ad hoc and is meant to be large enough to average over multiple boundary layer rolls but small enough to avoid large radial gradients. Hereafter, we will refer to the fluxes calculated from these localized horizontal averages as "grid-scale"
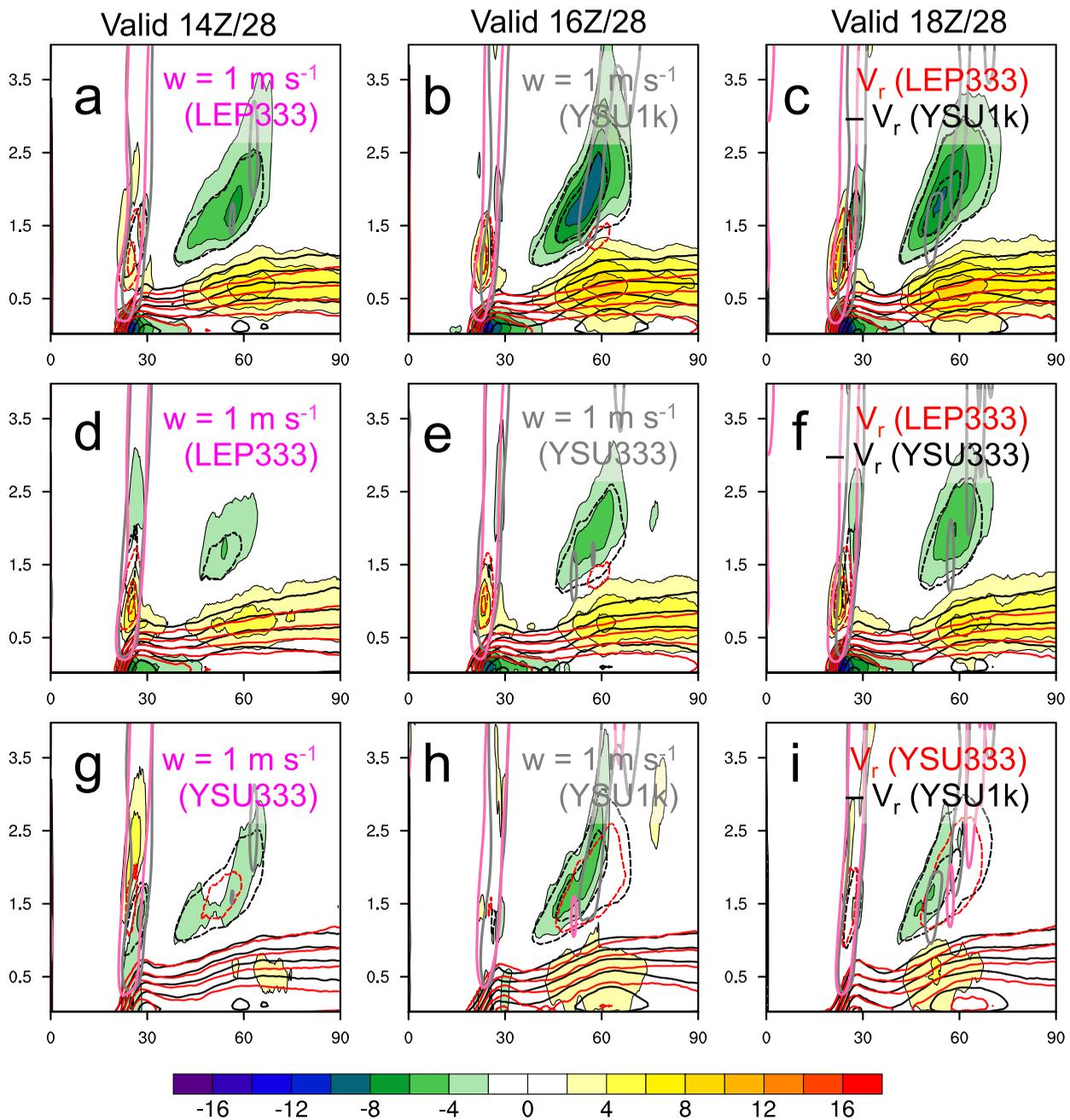
Figure 10. As in Figure 9, but for (top) LEP333 versus YSU1k, (middle) LEP333 versus YSU333, and (bottom) YSU333 versus YSU1k.

fluxes. Furthermore, for the sake of comparison, we also calculate these "grid-scale" fluxes for the PBL runs as well.

Fortunately, we can still calculate subgrid-scale fluxes in the same manner as any other simulation, though for the PBL runs, the subgrid-scale fluxes are supposed to represent the *entirety* of the turbulent momentum fluxes. Here we follow the approach of *Nolan et al.* [2009a] and use time tendencies from the PBL schemes to compute turbulent fluxes (see their section 6b). For the LEP runs, the SGS fluxes are calculated from equation (7) of *Mirocha et al.* [2010].

Figures 12 and 13 show the SGS vertical momentum fluxes, along with the sum of the SGS and "grid-scale" fluxes, averaged at different radii (30, 60, and 120 km) for the LEP runs and the PBL runs, respectively. The
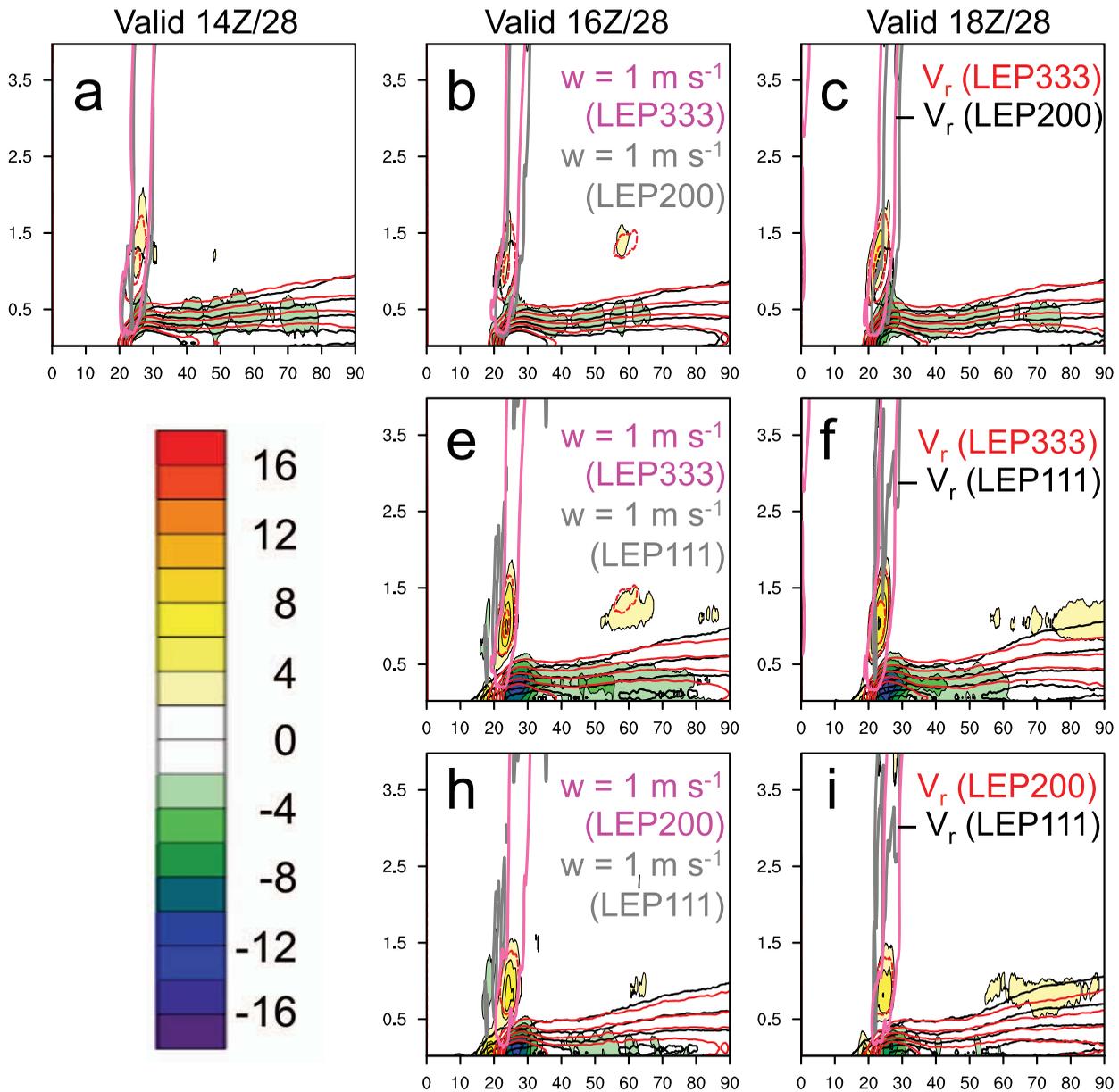
Figure 11. As in Figure 9, but for (top) LEP333 versus LEP200, (middle) LEP333 versus LEP111, and (bottom) LEP200 versus LEP111.

first point of note is that the fluxes change little over time (between 1400 UTC and 1800 UTC 28 August 2005). Additionally, at radii of 60 and 120 km (i.e., away from the eyewall), the *sum* of the SGS and "grid-scale" momentum fluxes are of comparable magnitude between the PBL and LEP runs. Furthermore, vertical momentum flux decreases with radius, which is to be expected because low-level vertical wind shear is strongest in the eyewall. Even more interesting are the *differences* between the runs, as detailed below.

The most obvious difference between the LEP runs and the PBL runs is the magnitude of the SGS vertical momentum fluxes in the lower part of the boundary layer. Just above the surface, the LEP runs have SGS vertical momentum fluxes about 4 times as strong as the PBL runs. Although it is not feasible to verify these simulated fluxes with observations, it should be noted that *Nolan et al.* [2009a] found that both the YSU and MYNN schemes significantly underestimate the vertical momentum flux just above the surface (their Figure 13a). Furthermore, *Green and Zhang* [2015] found in their idealized LES runs that for winds over the ocean
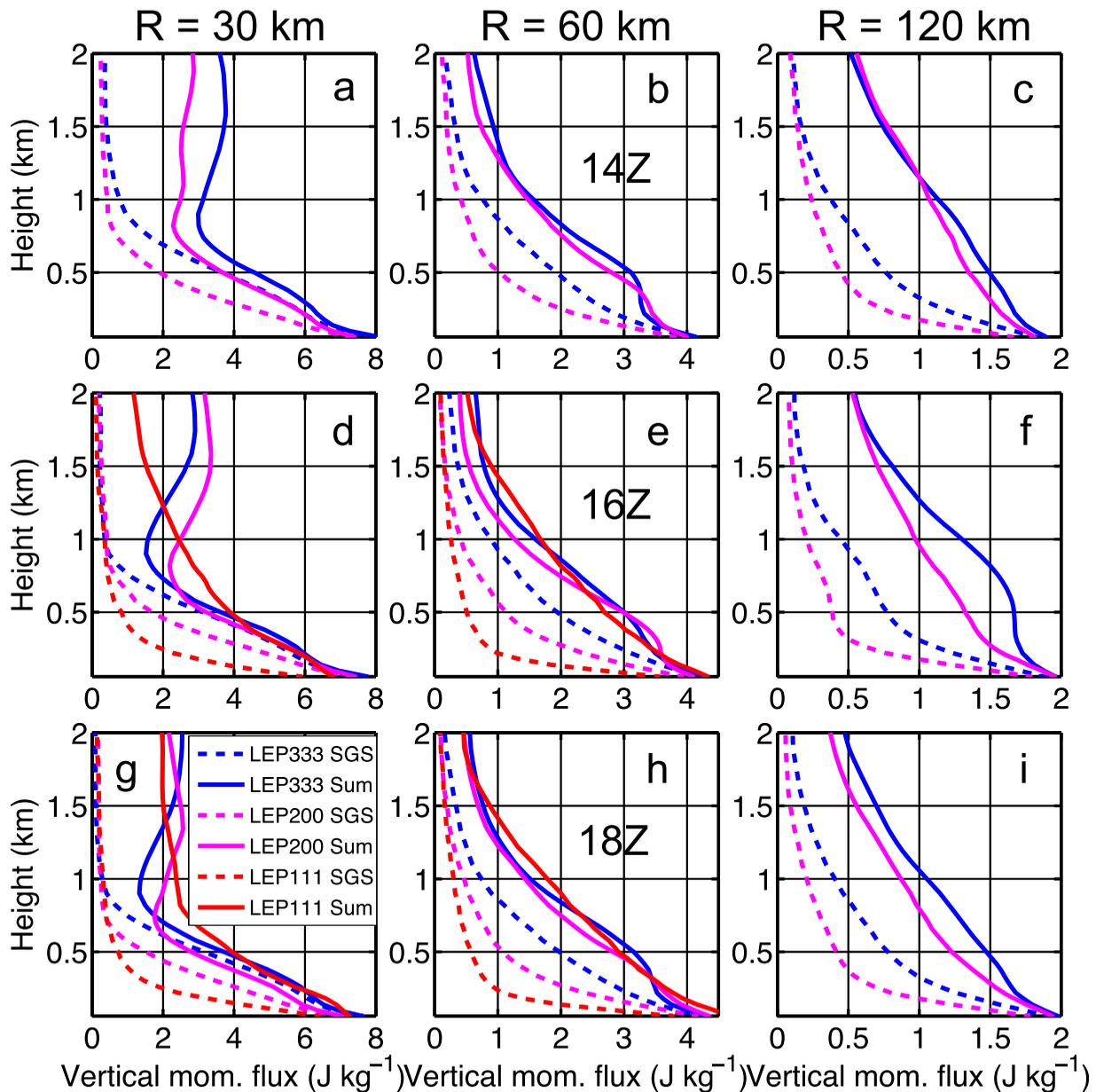
Figure 12. Vertical profiles of turbulent vertical momentum fluxes (in J kg^{-1}) for various LEP runs valid at (top) 1400 UTC, (middle) 1600 UTC, and (bottom) 1800 UTC 28 August 2005 at radii of (left) 30 km, (middle) 60 km, and (right) 120 km from TC center. Subgrid-scale turbulent vertical momentum fluxes (dashed) are plotted along with the sum of SGS fluxes and "grid-scale" turbulent vertical momentum fluxes (solid, see text).

of 70 m s^{-1} at a radius of 60 km from TC center, the magnitude of the SGS vertical momentum flux exceeded 4 J kg^{-1} (not shown), which is quite similar to the LEP runs at 60 km in this study (cf. Figures 12b, 12e, and 12h).

Figure 12 can also be used to evaluate whether or not the LEP runs are converging insofar as adequately resolving the large eddies is concerned. Reassuringly, with decreasing Δx, SGS vertical momentum fluxes become confined to closer to the surface; that said, there are still significant differences between LEP200 and LEP111 at heights above 500 m. Because of these differences, it is unlikely that the LEP runs have converged. An interesting result is that the sum of the SGS and "grid-scale" vertical momentum fluxes is fairly similar between the three LEP runs, which could mean that despite the differences in SGS fluxes, the LEP runs are having a similar impact on the rest of the TC—in other words, the evolution of the TC above the boundary layer may not be as sensitive to grid spacing in these simulations as might be expected.
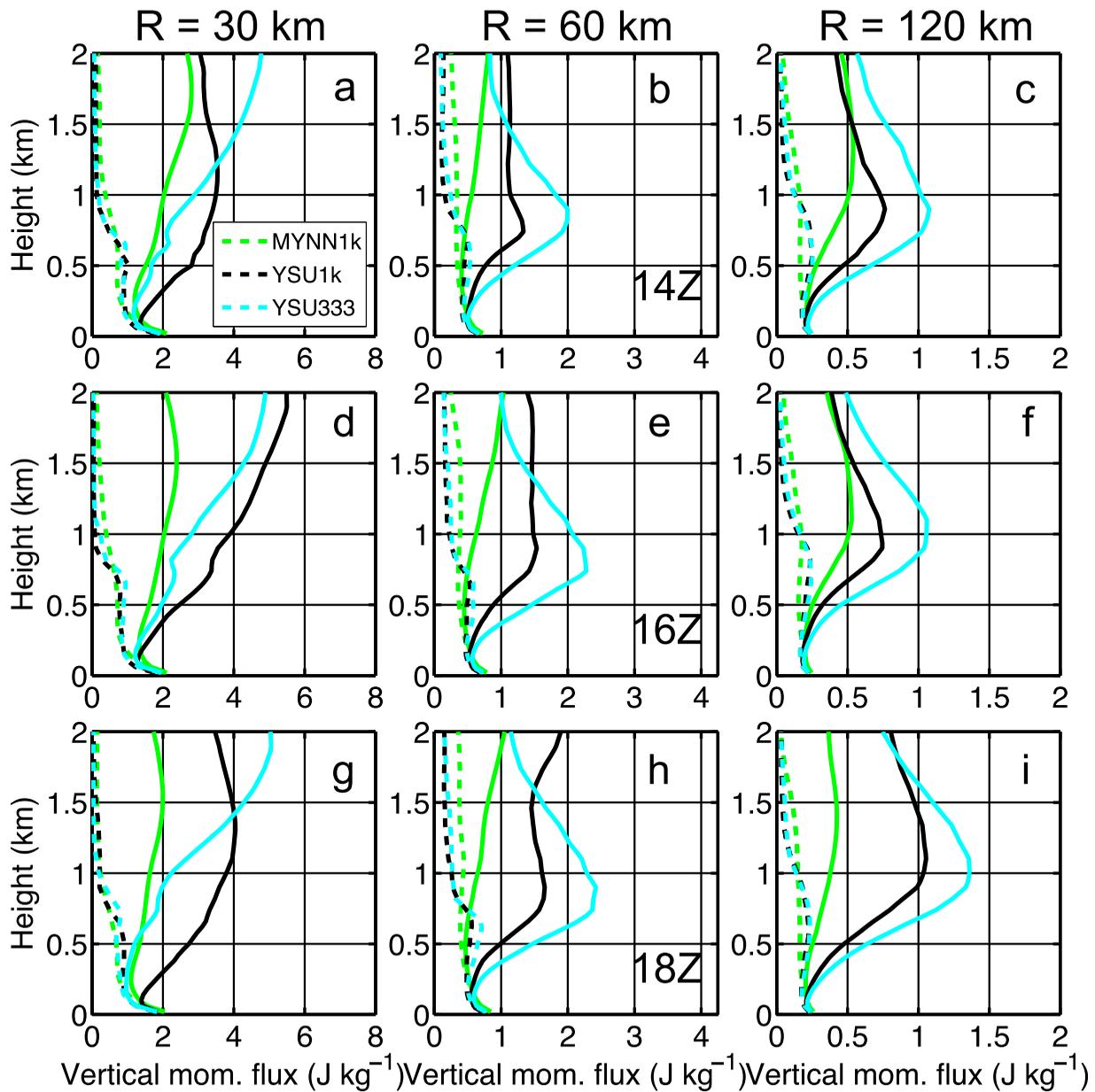
Figure 13. As in Figure 12, but for MYNN1k, YSU1k, and YSU333. Here, the dashed lines are vertical turbulent momentum fluxes diagnosed from the PBL scheme (see text).

As shown in Figures 12 and 13, there are substantial differences in the vertical momentum flux between the PBL runs and the LEP runs. To highlight these differences, Figure 14 shows the SGS and "grid-scale" vertical momentum fluxes (and their sum) for YSU333 and LEP333 at 1300 UTC (1 h after simulation start) and 1800 UTC. After the first hour (Figures 14a–14c), the "grid-scale" fluxes are still very similar between YSU333 and LEP333; the difference, clearly, is in the SGS fluxes. By 1800 UTC (Figures 14d–14f), the differences in the "grid-scale" fluxes are more substantial. Together, these results suggest that (at least initially) the differences in the SGS momentum flux are responsible for the different boundary layer structures in these two runs (Figures 10d–10f).

4. Discussion

With continued advances in computational power, TC simulations can be run at high enough resolution such that large boundary layer turbulent eddies start to become resolved [in what we call the
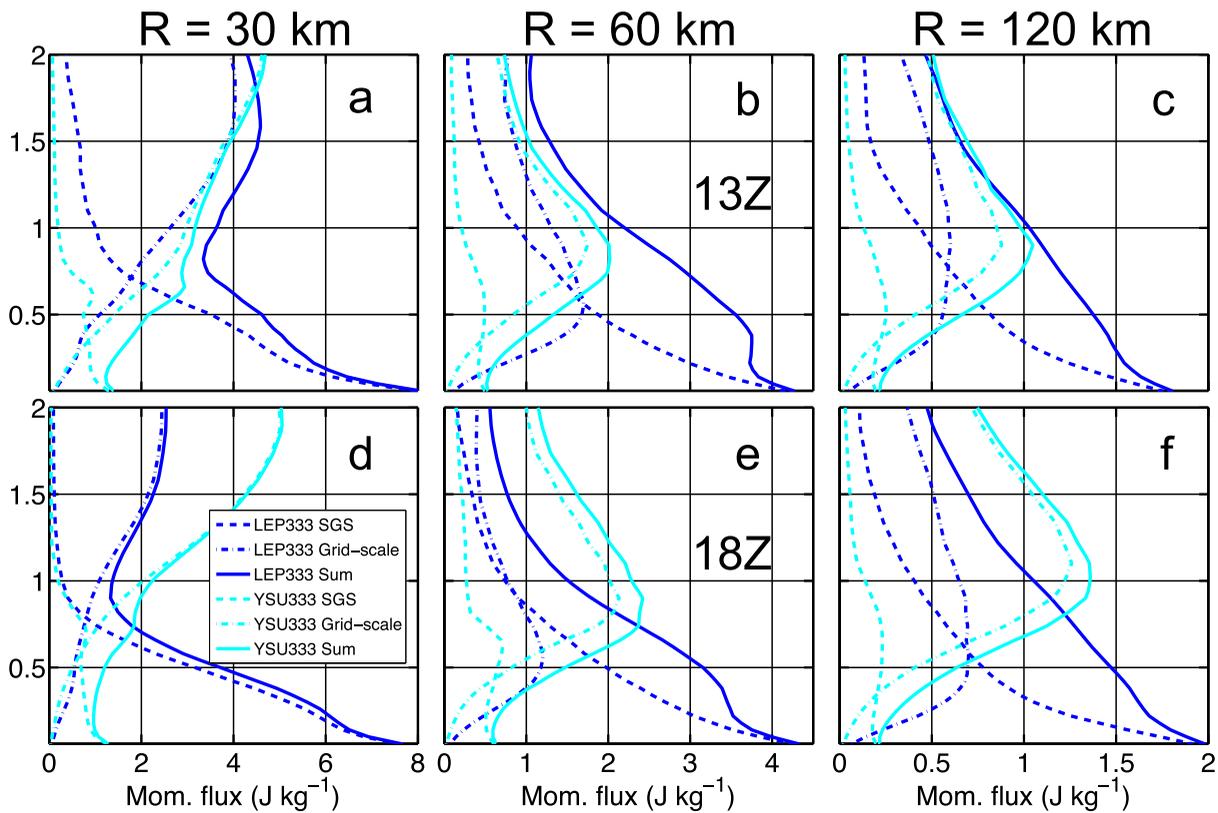
Figure 14. Similar to Figures 12 and 13, but for LEP333 (blue) and YSU333 (cyan); the "grid-scale" vertical turbulent momentum fluxes are also shown (dash-dotted lines). Top (bottom) row is valid 1300 UTC (1800 UTC) 28 August 2005.

"Large Eddy Permitting" (LEP) regime]. As TC research moves toward LEP, it is essential that various parameterizations of subgrid-scale (SGS) turbulence are well understood and tested in order to provide accurate, physically realistic TC simulations. For example, Rotunno et al. [2009] simulated the inner core of an idealized TC vortex using a TKE-based SGS scheme and only found small-scale turbulent structures at a horizontal grid spacing of $\Delta x = 62$ m; they write (p. 1786) that their "simulations strongly suggest that passing to a sub-100 m grid produces a simulation of an idealized tropical cyclone with at least partially resolved turbulence in the inner core." However, the present study runs counter to that statement: simulations using a nonlinear backscatter with anisotropy (NBA) SGS scheme (which has been shown to perform better than the TKE scheme at coarse resolutions [Mirocha et al., 2010]) exhibited such turbulent structures for Δx as coarse as 333.3333 m (Figures 2 and 3). While we did not have the computational resources necessary to perform additional simulations with the TKE SGS scheme (or any other SGS scheme), it is reasonable to believe that the NBA SGS allows for turbulent structures to appear at coarser Δx than what was found by Rotunno et al. [2009]. Regardless, the discrepancy between Rotunno et al. [2009] and this research raises an issue that should be addressed thoroughly in the future: how sensitive are TC LES (or LEP) runs to the choice of SGS scheme? And which SGS schemes are better suited for TC LES/LEP, particularly for 10^2 m $< \Delta x < 10^3$ m?

We also find (Figures 3 and 5) that the size of the simulated turbulence in the LEP runs is quite sensitive to Δx, with a coarser grid mesh (i.e., LEP333) yielding larger turbulent structures. Furthermore, the vertical momentum flux diagnosed by the NBA SGS becomes confined closer to the surface with increasing resolution (Figure 12). Together, these results indicate a strong sensitivity of the LEP runs to Δx. But at the same time, however, the *sum* of the vertical momentum flux from the NBA SGS and from a "grid scale" of 8 km remains essentially constant between the LEP runs (Figure 12), as does the secondary circulation (Figure 11) in the boundary layer [except right at the eyewall, although this may be due to the highly irregular eye shape of LEP111 (see discussion of Figure 6)]. This would imply that the LEP runs are not so sensitive to Δx,

which is clearly at odds with the beginning of this paragraph. A possible answer to this paradox is that while the *details* of the turbulence are highly sensitive to Δx in these simulations, the *net effect* of the boundary layer on the rest of the TC—and thus its subsequent evolution—is somewhat independent of grid spacing. Obviously, more rigorous testing—particularly by carrying out these integrations for longer than 6 h—is needed.

5. Concluding Remarks

For the first time, a Large Eddy Permitting (LEP) simulation of the inner core of a real tropical cyclone (Hurricane Katrina of 2005) has been performed, using the Weather Research and Forecasting model; subgrid-scale turbulence was parameterized by the nonlinear backscatter with anisotropy scheme (NBA) [*Mirocha et al.*, 2010]. Our LEP runs exhibited turbulent structures at horizontal grid spacing as coarse as $\Delta x = 333.3333$ m; in contrast, the idealized TC LES of *Rotunno et al.* [2009], which used a TKE SGS parameterization, did not find such structures until $\Delta x = 62$ m. A possible explanation for such different results is in the SGS scheme; regardless, exhaustive testing of SGS parameterizations for TC LES (or LEP) is necessary to determine the most suitable schemes for future research.

Although the LEP runs presented here (with $\Delta x = 333.3333$, 200, and 111.1111 m) all exhibited characteristics of turbulence in the boundary layer, the spatial scales of the turbulence were dependent on Δx. This result raises three possibilities (P. Zhu, personal communication, 2014). One is that Δx (as small as 111 m) is not in the inertial subrange and that further decreases in Δx will lead to LES convergence. A second possibility is that the simulated eddies do not behave like atmospheric eddies, in which case there will not be convergence to the inertial subrange regardless of the size of Δx. And finally, turbulence above the boundary layer (in the eyewall and in mesoscale rainbands) may not be resolved because vertical grid spacing Δz exceeds Δx at heights of 1.2 km (for LEP111), 3.2 km (for LEP200), and 6 km (for LEP333). All of that being said, however, the simulations presented herein yielded a similar *mean* boundary layer, especially so when compared against various mesoscale runs that parameterized boundary layer turbulence. Therefore, for the purposes of TC prediction—where the larger-scale features are more of interest than the structure of the boundary layer turbulence—using the NBA SGS scheme (or similar parameterizations designed to operate in the turbulent gray zone) may be worthwhile. The caveat is that our LEP runs were integrated forward for only 4–6 h. Thus, future research should carry out LES/LEP runs for longer periods of time (on the order of a few days) to determine if the larger-scale evolution of the simulated TC is as sensitive to Δx in the gray zone as it is to various PBL parameterizations and to Δx in the mesoscale. Additionally, our LEP runs were initialized when Katrina was already a very strong TC, so it would be interesting to see how LES/LEP handles the spin-up of a developing TC.

The LEP runs were also found to have vertical turbulent momentum fluxes in the lowest part of the boundary layer that were considerably larger than those of the PBL runs. While these large fluxes become confined closer and closer to the surface with decreasing Δx, there are very few flux observations at hurricane wind speeds [e.g., *French et al.*, 2007] against which the simulations can be verified. Another avenue of future research is to verify LES/LEP results against observations for TCs measured by the CBLAST field campaign [*Black et al.*, 2007].

With TC simulations moving into the turbulent gray zone, evaluating model performance against observed best track data becomes an issue. Traditionally, the model's maximum instantaneous 10 m wind speed at each output time has been used to verify against best track data. For mesoscale models, which only resolve the mean flow (i.e., sustained winds), such an approach is reasonable. But once the transient, small-scale turbulent wind *gusts*—which are much stronger than the mean flow—start to become resolved, the instantaneous maximum 10 m wind speed output by the model is no longer representative of the sustained winds recorded in best track data [e.g., *Nolan et al.*, 2009a]. Future endeavors into TC LES/LEP should consider how very high resolution, turbulence-resolving simulations can best be used to extract a "mean" intensity that can be used for both forecasting and verification purposes.

Finally, TC LES/LEP marks the convergence of two separate lines of study previously separated in scale due to computational constraints: TC research and turbulence (LES) research. Increased collaboration amongst scientists is necessary to ensure the appropriate tools (e.g., SGS scheme) are being used to answer the

appropriate questions (e.g., how does boundary layer turbulence impact the mean flow and evolution of a TC?). TC LES/LEP also has the potential to benefit those interested in hurricane risk, insofar as wind damage—particularly along the coastline—is concerned.

References

Bao, J.-W., S. G. Gopalakrishnan, S. A. Michelson, F. D. Marks, and M. T. Montgomery (2012), Impacts of physics representations in the HWRFX model on simulated hurricane structure and wind-pressure relationships, *Mon. Weather Rev.*, *140*(10), 3278–3299, doi:10.1175/MWR-D-11-00332.1.

Black, P. G., E. A. D'Asaro, T. B. Sanford, W. M. Drennan, J. A. Zhang, J. R. French, P. P. Niiler, E. J. Terrill, and E. J. Walsh (2007), Air-sea exchange in hurricanes: Synthesis of observations from the Coupled Boundary Layer Air-Sea Transfer Experiment, *Bull. Am. Meteorol. Soc.*, *88*(3), 357–374, doi:10.1175/BAMS-88-3-357.

Braun, S. A., and W.-K. Tao (2000), Sensitivity of high-resolution simulations of Hurricane Bob (1991) to planetary boundary layer parameterizations, *Mon. Weather Rev.*, *128*(12), 3941–3961, doi:10.1175/1520-0493(2000)129<3941:SOHRSO>2.0.CO;2.

Bryan, G. H. (2012), Effects of surface exchange coefficients and turbulence length scales on the intensity and structure of numerically simulated hurricanes, *Mon. Weather Rev.*, *140*(4), 1125–1143, doi:10.1175/MWR-D-11-00231.1.

Bryan, G. H., J. C. Wyngaard, and J. M. Fritsch (2003), Resolution requirements for the simulation of deep moist convection, *Mon. Weather Rev.*, *131*(10), 2394–2416, doi:10.1175/1520-0493(2003)131<2394:RRFTSO>2.0.CO;2.

Bryan, G. H., D. P. Stern, and R. Rotunno (2014), A framework for studying the inner core of tropical cyclones using large eddy simulation, paper presented at 31st Conference on Hurricanes and Tropical Meteorology, *Am. Meteorol. Soc.*, San Diego, Calif.

Donelan, M. A., B. K. Haus, N. Reul, W. J. Plant, M. Stiassnie, H. C. Graber, O. B. Brown, and E. S. Saltzman (2004), On the limiting aerodynamic roughness of the ocean in very strong winds, *Geophys. Res. Lett.*, *31*, L18306, doi:10.1029/2004GL019460.

Emanuel, K. A. (1986), An air-sea interaction theory for tropical cyclones. Part I: Steady-state maintenance, *J. Atmos. Sci.*, *43*(6), 585–604, doi:10.1175/1520-0469(1986)043<0585:AASITF>2.0.CO;2.

Emanuel, K. A. (1995), Sensitivity of tropical cyclones to surface exchange coefficients and a revised steady-state model incorporating eye dynamics, *J. Atmos. Sci.*, *52*(22), 3969–3976, doi:10.1175/1520-0469(1995)052<3969:SOTCTS>2.0.CO;2.

Fang, J., and F. Zhang (2012), Effect of beta shear on simulated tropical cyclones, *Mon. Weather Rev.*, *140*(10), 3327–3346, doi:10.1175/MWR-D-10-05021.1.

French, J. R., W. M. Drennan, J. A. Zhang, and P. G. Black (2007), Turbulent fluxes in the hurricane boundary layer. Part I: Momentum flux, *J. Atmos. Sci.*, *64*(4), 1089–1102, doi:10.1175/JAS3887.1.

Green, B. W., and F. Zhang (2013), Impacts of air-sea flux parameterizations on the intensity and structure of tropical cyclones, *Mon. Weather Rev.*, *141*(7), 2308–2324, doi:10.1175/MWR-D-12-00274.1.

Green, B. W., and F. Zhang (2014), Sensitivity of tropical cyclone simulations to parametric uncertainties in air-sea fluxes and implications for parameter estimation, *Mon. Weather Rev.*, *142*(6), 2290–2308, doi:10.1175/MWR-D-13-00208.1.

Green, B. W., and F. Zhang (2015), Idealized large eddy simulations of a tropical cyclone-like boundary layer, *J. Atmos. Sci.*, doi:10.1175/jas-d-14-0244, in press.

Hong, S.-Y., Y. Noh, and J. Dudhia (2006), A new vertical diffusion package with an explicit treatment of entrainment processes, *Mon. Weather Rev.*, *134*(9), 2318–2341, doi:10.1175/MWR3199.1.

Kepert, J. D. (2013), How does the boundary layer contribute to eyewall replacement cycles in axisymmetric tropical cyclones?, *J. Atmos. Sci.*, *70*(9), 2808–2830, doi:10.1175/JAS-D-13-046.1.

Kepert, J. D., and Y. Wang (2001), The dynamics of boundary layer jets within the tropical cyclone core. Part II: Nonlinear enhancement, *J. Atmos. Sci.*, *58*(17), 2485–2501, doi:10.1175/1520-0469(2001)058<2485:TDOBLJ>2.0.CO;2.

Mirocha, J. D., J. K. Lundquist, and B. Kosović (2010), Implementation of a nonlinear subfilter turbulence stress model for large-eddy simulation in the Advanced Research WRF Model, *Mon. Weather Rev.*, *138*(11), 4212–4228, doi:10.1175/2010MWR3286.1.

Nakanishi, M., and H. Niino (2004), An improved Mellor-Yamada level-3 model with condensation physics: Its design and verification, *Boundary Layer Meteorol.*, *112*(1), 1–31, doi:10.1023/B:BOUN.0000020164.04146.98.

Nakanishi, M., and H. Niino (2012), Large-eddy simulation of roll vortices in a hurricane boundary layer, *J. Atmos. Sci.*, *69*(12), 3558–3575, doi:10.1175/JAS-D-11-0237.1.

Nolan, D. S., J. A. Zhang, and D. P. Stern (2009a), Evaluation of planetary boundary layer parameterizations in tropical cyclones by comparison of in situ observations and high-resolution simulations of Hurricane Isabel (2003). Part I: Initialization, maximum winds, and the outer-core boundary layer, *Mon. Weather Rev.*, *137*(11), 3651–3674, doi:10.1175/2009MWR2785.1.

Nolan, D. S., D. P. Stern, and J. A. Zhang (2009b), Evaluation of planetary boundary layer parameterizations in tropical cyclones by comparison of in situ observations and high-resolution simulations of Hurricane Isabel (2003), Part II: Inner-core boundary layer and eyewall structure, *Mon. Weather Rev.*, *137*(11), 3675–3698, doi:10.1175/2009MWR2786.1.

Rotunno, R., and G. H. Bryan (2014), Effects of resolved turbulence in a large eddy simulation of a hurricane, paper presented at 31st Conference on Hurricanes and Tropical Meteorology, *Am. Meteorol. Soc.*, San Diego, Calif.

Rotunno, R., Y. Chen, W. Wang, C. Davis, J. Dudhia, and G. J. Holland (2009), Large-eddy simulation of an idealized tropical cyclone, *Bull. Am. Meteorol. Soc.*, *90*(12), 1783–1788, doi:10.1175/2009BAMS2884.1.

Ryglicki, D. R., and R. E. Hart (2014), Evaluating different methods for determining the vertical structure of tropical cyclones in mesoscale models, paper presented at 31st Conference on Hurricanes and Tropical Meteorology, *Am. Meteorol. Soc.*, San Diego, Calif.

Skamarock, W. C., J. B. Klemp, J. Dudhia, D. O. Gill, D. M. Barker, M. G. Duda, X.-Y. Huang, W. Wang, and J. G. Powers (2008), A description of the Advanced Research WRF version 3, *NCAR Tech. Note, NCAR/TN-475+STR*, 113 pp. [Available at http://www2.mmm.ucar.edu/wrf/users/docs/arw_v3.pdf.]

Stern, D. P., and G. H. Bryan (2014), The structure and dynamics of coherent vortices in the eyewall boundary layer of tropical cyclones, paper presented at 31st Conference on Hurricanes and Tropical Meteorology, *Am. Meteorol. Soc.*, San Diego, Calif.

Sullivan, P. P., J. C. McWilliams, and C.-H. Moeng (1994), A subgrid-scale model for large-eddy simulation of planetary boundary-layer flows, *Boundary Layer Meteorol.*, *71*(3), 247–276, doi:10.1007/BF00713741.

Tao, D., and F. Zhang (2014), Effect of environmental shear, sea-surface temperature, and ambient moisture on the formation and predictability of tropical cyclones: An ensemble-mean perspective, *J. Adv. Model. Earth Syst.*, *6*, 384–404, doi:10.1002/2014MS000314.

Wang, X., Y. Ma, and N. E. Davidson (2013), Secondary eyewall formation and eyewall replacement cycles in a simulated hurricane: Effect of the net radial force in the hurricane boundary layer, *J. Atmos. Sci.*, *70*(5), 1317–1341, doi:10.1175/JAS-D-12-017.1.

Wang, Z. (2014), Characteristics of convective processes and vertical vorticity from the tropical wave to tropical cyclone stage in a high-resolution numerical model simulation of Tropical Cyclone Fay (2008), *J. Atmos. Sci.*, *71*(3), 896–915, doi:10.1175/JAS-D-13-0256.1.

Weng, Y., and F. Zhang (2012), Assimilating airborne Doppler radar observations with an ensemble Kalman filter for convection-permitting hurricane initialization and prediction: Katrina (2005), *Mon. Weather Rev.*, *140*(3), 841–859, doi:10.1175/2011MWR3602.1.

Wyngaard, J. C. (2004), Toward numerical modeling in the ''terra incognita,'' *J. Atmos. Sci.*, *61*(14), 1816–1826, doi:10.1175/1520-0469(2004)061<1816:TNMITT>2.0.CO;2.

Zhu, P. (2008), Simulation and parameterization of the turbulent transport in the hurricane boundary layer by large eddies, *J. Geophys. Res.*, *113*, D17104, doi:10.1029/2007JD009643.